NASA TECHNICAL MEMORANDUM

NOZZLE PERFORMANCE MEASUREMENT ON UNDERWING NACELLES OF AN F-106 UTILIZING CALIBRATED ENGINES AND LOAD CELLS

by Harold W. Groth
Lewis Research Center
Cleveland, Ohio

NOZZLE PERFORMANCE MEASUREMENT ON UNDERWING NACELLES ON AN
F-106 UTILIZING CALIBRATED ENGINES AND LOAD CELLS

Harold W. Groth
National Aeronautics and Space Administration
Lewis Research Center
Cleveland, Ohio

ABSTRACT

A flight research program is underway at the Lewis Research Center to study installation effects on turbojet engine exhaust nozzles over a range of flight Mach number from 0.60 to 1.30. Two J85-13 afterburning turbojet engines were mounted in underwing nacelles. Exhaust nozzle propulsion efficiency is being measured using load cells, calibrated engines, and flight calibrated nacelle tare forces. Reference nozzles of known performance were used to determine nacelle tare forces. Analysis of flight calibration data shows that the system is capable of determining nozzle efficiency to a one-sigma randomerror of ±1.5 percent.

INTRODUCTION

A flight research program is being conducted at the Lewis Research Center to study airframe installation effects on underwing-nacelle-mounted turbojet engine exhaust nozzles at flight Mach numbers from 0.60 to 1.3. This program permits large scale testing in the transonic speed range where wind tunnels suffer from wall interference problems due to blockage effects and shock reflections. The primary objective of the program is to evaluate the installed efficiencies of various nozzle types for both supersonic cruise and supersonic dash aircraft.[1] To do this it is necessary to measure accurately engine operating parameters so that the internal thrust can be determined. In addition, a measurement of the nozzle thrust minus drag must be obtained.

The nozzle internal ideal thrust can be obtained by using the gas generator method (c.f., ref. 2). In this method ground calibrations of the engine and afterburner are made. Inflight measurements of various temperatures and pressure are obtained and correlated with the ground calibrations to obtain the internal nozzle operating conditions. An alternate approach to determine nozzle internal gross thrust is to use a traversing rake at the nozzle exit. Results obtained by this method are reported in Ref. 3 for a turbojet engine and in Ref. 4 for a turbofan engine. In either case additional information is required regarding the flow field resulting from the interaction of the internal and external flows in evaluating the overall thrust and drag characteristics of a complete exhaust system. For simple exhaust system concepts it may be sufficient in determining nozzle drag just to measure the pressure forces acting upon the exterior surfaces of the nozzle boattail. However for more complex concepts (such as those utilizing auxiliary inlets) many more details of the flow influence the nozzle thrust minus drag propulsive force. The problem is further complicated when the external flow is distorted by the airframe installation effects. As a result it may not be practical to determine nozzle drag from pressure measurements since an excessive number of such measurements would be required.

The technique to be described in this paper uses the gas generator method to determine the nozzle ideal internal thrust and a load cell to measure the nozzle thrust minus drag. An F106 aircraft (fig. 1) was modified to permit installation of two nacelle-mounted J85-GE-13 afterburning turbojet engines. The nacelles were attached to the wings by links which permit forces parallel to the nacelle axis to be measured by a load cell. A calibrated reference nozzle permitted separation of drag forces on the forward part of the nacelle from the nozzle forces for the series of flights discussed in this paper. The general approach is outlined in Fig. 2. Ground calibrations were made of the engine, reference nozzle, and load cell. These calibrations were used to obtain nacelle tare drag forces in flight which finally permitted the research nozzle installed efficiency to be evaluated.

The purpose of this paper is to describe the thrust measurement system, data acquisition system, and to present the results of the calibration phase of the program. Special attention will be given to the accuracy that can be expected in flight using this technique with ground calibrations of engines and nozzles such as those presented in Refs. 5 and 6. An analysis of the expected errors was performed and it will be compared to flight results.

FLIGHT FACILITY

Installation

The underwing nacelles had normal shock inlets and calibrated J85-GE-13 turbojet engines as shown in Fig. 3. Also shown on Fig. 3 are the front and rear links and the location of the load cell. Secondary air to cool the engine and afterburner was supplied from the inlet and controlled at the periphery of the compressor face by a rotary valve.

Thrust Measurement System

The nacelle support system, consisted of a front link, a rear link, and a load cell assembly located between the two links. The front and rear links were each attached to a wing fitting and a nacelle fitting with low friction bearings. The front and rear links transferred all loads acting on the nacelle directly to the wing except loads acting in the direction of the nacelle thrust axis. These loads were transferred to the wing through the load cell.

The load cell was a miniature type containing a semiconductor strain-gage bridge and was vented so that no cell tare force was encountered due to pressure variations. It was attached to a nacelle fitting through spherical bushings.

In order to compensate the load cell for forces due to acceleration and nacelle weight com-

1

ponents along the nacelle axis, an accelerometer output was combined with the load cell output as shown schematically in Fig. 4. The setting of the potentiometer determined the portion of the servo accelerometer signal which was subtracted from the load cell signal to obtain the net thrust minus drag output. The potentiometer was adjusted on the ground to a position which made this output read zero, since the output load cell should be zero at static conditions. Low pass filters were incorporated in both the load cell and accelerometer circuits to attenuate frequencies higher than the natural frequency of the nacelle support system. In addition, the thrust measurement was recorded 48 times during a 11.52 second data scan. .

To maintain a constant temperature environment, the accelerometer mounting block and both ends of the load cell were equipped with heaters and thermoswitches, and the accelerometer and load cell were wrapped with insulation. The temperature of these units was maintained within 11 K (20° F) or 311 K (100° F)

In ground calibrations, the accuracy of the load cell reading compared with known forces applied to the nacelle was within ±0.1 percent of full scale. This included hysteresis, nonlinearity, and data recording system errors, but did not include errors due to changes in temperature or acceleration compensation. The overall one sigma system accuracy is estimated as ±0.25 percent of full scale.

Airborne Data Acquisition System

The data system was designed to achieve an inherently high accuracy and repeatability. Wherever possible, the transducers, instruments, and techniques used were those which had proven to give consistently accurate results with good reliability in other programs. Also incorporated in the program was the pre-selection of transducers to obtain the best units of a type, and thermostatically-controlled electrical heating of the transducers was used to minimize thermal drift during flight.

The data acquisition system, as shown in Fig. 5 consisted of a system to multiplex and record quasistatic data in digital form on magnetic tape, and a system to record dynamic data and variations in flight parameters in FM analog form on a second magnetic tape. Major components of the data system are illustrated in Fig. 6.

Static pressures were sampled by means of scanivalves. The scanivalve unit contained a solenoid-actuated rotating pressure passage which sequentially connected 48 pressure lines to a single transducer. Ten scanivalves located in two nacelles provided for a capacity of 480 pressure measurements.

Each of the pressures was recorded only once during a data scan. Thermocouples, potentiometers, and other transducer outputs were sampled and recorded six times during a scan. The load cell outputs were sampled 48 times during the data scan of 11.52 seconds. The total scan included 1152 words.

The maximum error specification for the digital data system required that 99.73 percent of the samples (three sigma, with a normal distribution)

would be within ±0.34 percent of full scale. This included errors from all sources (ambient temperature and pressure, non-linearity, gain inaccuracy, zero offset, drift, noise, etc.) except transducer error. To check this accuracy, a reference voltage was recorded by the data system during each scan. The maximum error of this reading from data recording during research flights was within ±0.1 percent of full scale.

Method of Thrust Measurement

The parameter of primary interest in the research nozzle test program is the installed nozzle efficiency which is defined as follows:

$$\eta = \frac{(T - D)_{nozzle}}{F_{ip}} \qquad (1)$$

where

$(T - D)_{nozzle}$ installed thrust minus drag of the nozzle

F_{ip} ideal thrust of the primary jet

The ideal thrust is obtained from engine calibrations[6] utilizing the gas generator method. The airflow is obtained from a typical calibration of corrected airflow versus corrected speed, fuel flows are metered for both reheat and non-reheat, and temperatures and pressures at the discharge of the turbine are directly measured. For reheat conditions additional calibrations for afterburner pressure drop and temperature rise were made. A typical plot of afterburner temperature rise vs. afterburner fuel-air ratio is shown in Fig. 7. Figure 8 shows this inlet, engine, and nozzle combination in the ground test facility. From these conditions and calibrations the ideal primary thrust is determined.

The $(T - D)_{nozzle}$ is obtained from the load cell system in the following manner. The load cell measures the sum of all forces acting on the nacelle. These forces are shown on Fig. 9 and are summed as follows:

$$F_{l.c.} + m_n(a + g \sin \theta) = (T - D)_{nozzle}$$

$$-(D_{ram} + D_{add} + D_{strut} + D_{fnac} + D_{cowl} + D_{bump}) \quad (2)$$

The summation of terms within the brackets is the total of all drag forces (tare force) on the strut and nacelle forward of station 127.68. This is the nacelle-nozzle juncture station for all research nozzles. The term $m_n(a + g \sin \theta)$ is obtained from the output of the accelerometer. When this is combined with raw load cell reading, $F_{l.c.}$, the left hand side of the equation is referred to as the compensated load cell reading. The $(T - D)_{nozzle}$ is then obtained by knowing the tare and the value of the compensated load cell.

The tare forces have been empirically obtained over the range of Mach number, mass-flow ratio, and engine power settings by installing reference nozzles on each nacelle and flying calibration flights. These nozzles were simple, cylindrical ejectors with flat external base areas and whose internal thrust had been calibrated and whose ex-

ternal drag could be easily measured. The internal thrust of each reference nozzle was determined by correlation with a nozzle thrust coefficient, C_f. Here again it was necessary to use the gas generator to establish flow conditions at the engine primary exit. Figure 10 shows the functional relationship of C_f to nozzle pressure ratio for a given corrected secondary weight flow of 0.04, for various effective primary nozzle areas. The secondary air flow was determined from valve open area and pressure drop characteristics. The calibrations were made inflight using ejector nozzle pumping characteristics determined in a ground calibration of the nozzle.

The external drag of the reference nozzles was found by pressure measurement on the known base area and by calculation of a skin friction drag. Skin friction was calculated using flat plate theory with the skin friction coefficient defined as $C_f = 0.075/Re^{1/5}$.

RESULTS

The primary objectives of the in-flight calibration were to obtain the nacelle tare drags for later use in research flights and to assess the accuracy of the thrust measuring system.

Typical results are presented in Fig. 11. Nacelle tare coefficient is plotted versus inlet capture mass flow ratio. The data of Fig. 11 were obtained at a flight Mach number of 0.90±0.02. Data were corrected to Mach 0.90 by using the measured sensitivity of tare coefficient to Mach number in an iterative process. As can be seen on Fig. 11 the tare coefficient appears to be a linear function of mass flow ratio. This linear relationship existed for all Mach numbers. A least squares curve fit was made of all military power data for each nacelle at discrete Mach numbers. Since little difference was observed between the left and right nacelle tare coefficients they were combined into one function which was an average of the left and right values.

Cross plots of these data were made at discrete Mach numbers from 0.60 to 1.30, at a mass-flow ratio of 0.82, to obtain tare coefficients as a function of Mach number, Fig. 12. The sensitivity of tare coefficient to m/m_0 was also determined and is presented in Fig. 13. Thus the tare coefficient can be obtained by determining the value at the desired Mach number from Fig. 12 and correcting that value to the correct m/m_0 by using the sensitivity from Fig. 13.

As can be seen on Fig. 11, the scatter of data or deviation from the line becomes greater when the engine is afterburning. Only the left engine afterburning data are presented but the right engine data exhibits the same tendency. The afterburning error is evidenced as a bias in tare coefficient. That is, all the minimum reheat data lies lower than the military data and the maximum afterburner data lies above the military. Therefore, it is felt that these apparent biases in afterburning are the result of errors in the determination of reference nozzle thrust coefficients during calibration and possible inaccuracies in the engine afterburner calibrations. An inaccuracy in nozzle thrust coefficient in maximum afterburning of 1 percent produces a 3.64 percent error in

tare coefficient. Both of these effects combine to produce the apparent shift in drag coefficient during afterburner operation. Therefore, these biases are not taken into account in determining nacelle tare, and the curves of Fig. 11 are based on military power data only.

STATISTICAL RESULTS

An analysis of flight data was made to determine the random error of the tare forces, which indicates the repeatability of the system. The random error was evaluated for all military power data points used to determine the tare coefficient as a function of m/m_0. This calculation was made at various discrete Mach numbers where data were available. The results are shown in Fig. 14. The standard deviation of the data is defined as follows:

$$\sigma = \sqrt{\frac{\sum_{i=1}^{n} y_i^2}{n}} \qquad (3)$$

where

σ standard deviation

y_i difference between experimental tare coefficient data point and the curve fit of data

n number of data points

Figure 14 shows the standard deviation as a percent of tare plotted versus Mach number. Also shown as a solid line is the level of error in tare necessary to produce a one-percent error in nozzle thrust minus drag. The standard deviation of all the data is shown to be within a one percent error in thrust minus drag.

The probability distribution of all military power data (340 points) over the entire Mach range was compared to that of a normal distribution with a mean error in drag coefficient of -1.00×10^{-4} and a standard deviation of 20.45×10^{-4}. This is the mean and standard deviation calculated from the data. If the data were perfectly curve fit by a least squares method the mean error would be zero. However the curves used were the average of curve fits of the left and right nacelles. A plot of these distributions is shown in Fig. 15. The sample distribution is nearly normal but has a greater concentration of data in the region of low random error than the normal distribution. The sample has 72 percent of the data less than one sigma where-as the normal distribution includes 68 percent of the data less than one sigma.

ERROR ANALYSIS

An error analysis was performed to estimate the random error in determining nacelle drag, and nozzle efficiencies. The method used the root-sum square of the random errors contributed by each measured parameter.

3

$$E = \sqrt{\sum_{i=1}^{n}\left[(C_i)\left(\frac{\Delta X_i}{X_i}\right)\right]^2} \qquad (4)$$

where

E   estimated random error for one standard deviation

C_i influence coefficient of any given measurement

$\dfrac{\Delta X_i}{X_i}$ estimated accuracy of any given measurement for one standard deviation

n   total number of measurements influencing desired result

Influence coefficients were found for each measured parameter using a computer technique. Each parameter in the data computation program which influenced nacelle drag, or nozzle ideal thrust was perturbed a known amount while all other such parameters were held constant. A flight data point was used as the base measurement. The change in nacelle tare coefficient, or ideal thrust, due to these perturbations was then computed. From these changes the influence coefficients were calculated for both military power settings and for afterburning. Included in the influence coefficient analysis were changes due to possible errors in ground calibrations of engine airflow, secondary airflow, afterburner pressure drop, afterburner temperature rise, and nozzle thrust coefficient.

The estimates of measurement accuracy were obtained during calibrations of the various instruments and empirical knowledge of similar measurements. These estimates were combined with the accuracy of the data system to estimate the overall accuracy of the measurement. For determination of the ground calibration accuracies the basic data were analyzed and the random error of the data were calculated. The one sigma values of estimated measurement accuracy are shown in table 1.

Table 2 summarizes the results of the error analysis for a military power setting at Mach 0.90. All parameters affecting nacelle tare force and nozzle ideal thrust are listed in the first column. They are subdivided into three categories; measured engine and nozzle parameters, calibrated parameters, and measured free stream parameters. Influence coefficients which affect the tare coefficient are shown in the second column. The tare coefficient is the primary end result of the present system calibration. The third column shows the influence coefficient for computed nozzle ideal thrust which is used to compute nozzle efficiency. This efficiency is the parameter of most interest when the system is used to measure performance of a research nozzle. The measurement accuracy column was obtained from the overall measurement accuracies of table 1 corrected for the proper range of full scale error. When the accuracy was estimated for a calibration

parameter, such as nozzle thrust coefficient, the random scatter in the basic calibration data was used. In the final two columns the influence coefficients are combined with the estimated accuracies to obtain the contribution to the final tare coefficient and to nozzle ideal thrust. Both the tare coefficient and nozzle ideal thrust are most affected by compressor face total pressure measurement. The random error estimate for the tare coefficient was ±3.9 percent and for the nozzle ideal thrust it was ±1.1 percent.

Tables 3 and 4 show the results of the error analysis for minimum and maximum reheat respectively, also at Mach 0.90. For both power settings the nozzle ideal thrust is most affected by measurement errors in compressor face total pressure, but the tare coefficient is most affected by possible calibration errors in the reference nozzle thrust coefficient. This greater error of tare coefficient from that at military power setting is due in part to the greater thrust level in afterburning and also to the calibration accuracy assessed to the nozzle thrust coefficient. The expected random error in tare coefficient for minimum and maximum reheat was ±5.7 percent and ±6.5 percent respectively, while the expected random error for nozzle ideal thrust was ±1.1 percent and ±1.2 percent.

The results of the error analysis of tare coefficient and nozzle ideal thrust were used to calculate the expected error in determining the efficiency of research nozzles. This calculation is summarized in tables 5, 6, and 7. The three parameters used to calculate nozzle efficiency are tare, load cell force, and nozzle ideal thrust. Again influence coefficients were found for these three parameters and were combined with accuracy values. The accuracy values were taken from the tables (E-values). A single accuracy value of ±3.9 percent for tare coefficient was used for all power settings since tare was determined by military data only. The expected random error in nozzle efficiencies were calculated to be; ±2.5 percent for military, ±1.87 percent for minimum reheat, and ±1.81 percent for maximum reheat.

A comparison of random error of flight data with the estimated accuracies of the error analysis showed that the flight data at Mach 0.90 (fig. 13) exhibited a random error of ±1.5 percent in tare coefficient whereas the estimate was ±3.9 percent. This difference indicates conservatism in the estimates of measurement and calibration accuracies.

Another comparison of maximum afterburning data showed a random flight error in tare coefficient of ±4.0 percent whereas the estimated error was ±6.5 percent. Here too, the estimate showed conservatism.

Since the tare coefficient shows less random error in flight than the estimated errors it is assumed that the ideal thrust accuracy in flight will also be better than estimated. If just the exhibited flight scatter of ±1.5 percent is used in a recalculated nozzle efficiency error estimate instead of the original value of ±3.9 percent and the same ideal thrust accuracy is used, the error estimates are reduced to ±1.5 percent for military, ±1.4 percent for minimum reheat, and ±1.3

percent for maximum reheat. These estimates are probably still conservative because the estimated errors in ideal thrust were not reduced from the original estimate. These calculations are also summarized in tables 5, 6, and 7, when the experimental nacelle parameter is used in the calculations rather than the estimated value.

This error analysis was made at only Mach 0.90 because this Mach number is of prime interest in the research program and because more data was available at this condition for analysis. The error in efficiency should vary somewhat with Mach number if the experimental values of tare coefficient are used for an error estimate. The error should vary according to relationships shown in Fig. 13. The error should be greater for Mach numbers less than 0.90 and smaller at Mach numbers greater than 0.90.

It should also be recognized that the errors quoted are one sigma values so that they are only applicable to 68 percent of the data taken. It would be necessary to take many data points at each condition to be confident that the random error of ± 1.5 percent in nozzle efficiency would be approached.

CONCLUSIONS

It was demonstrated that the thrust measuring system installed on F106B aircraft is capable of determining nacelle tare forces whose repeatability affects nozzle thrust minus drag no greater than ± 1 percent for military power setting. This was accomplished by using ground calibrations of engine airflow, afterburner pressure drops and temperature rises, nozzle thrust coefficient, and a load cell.

An error estimate of expected values of nozzle efficiency was made using the experimental value of tare coefficient random error of ± 1.5 percent at a Mach number of 0.90. This estimate indicated an expected random error of within ± 1.5 percent in nozzle efficiency for all power settings, for a one sigma deviation, or for 68 percent of the data.

SYMBOLS

A_8	primary nozzle exit effective area
a	nacelle axial acceleration
C_F	ejector thrust coefficient, $T/P_8 A_8$
C_f	skin friction drag coefficient
D	nozzle drag
D_{add}	inlet additive drag
D_b	base drag of ejector
D_{bump}	pressure drag on reward facing nacelle step
D_{cowl}	pressure drag and skin friction drag on inlet cowl
D_f	skin friction drag on ejector
$D_{f_{nac}}$	skin friction drag on nacelle
D_{ram}	ram drag, mV_O
D_{strut}	pressure and skin friction drag on strut fairing
$F_{l.c.}$	force measured by load cell
$(F_{l.c.})_{compensated}$	force measured by load cell compensated for acceleration and angle of attack
g	acceleration of gravity
M_O	free-stream Mach number
m	mass of air captured by inlet
m_n	mass of nacelle
m_o	mass of air that could be captured by inlet if full stream tube were swallowed. It is based upon free-stream density and velocity and inlet capture area having a diameter of 37.37 cm (14.715 in.)
P	total pressure
p	static pressure
P_8	total pressure at primary nozzle
p_9	static pressure, internal at ejector exit
q	free-stream dynamic pressure
Re	Reynolds number
S	reference area 2.2 m^2 (23.9 ft^2)
T	ejector internal thrust
T_5	total temperature at turbine discharge
T_8	total temperature at primary nozzle
V_O	free stream velocity
η	nozzle efficiency parameter $(T - D)_{nozzle}/F_{ip}$
θ	nacelle angle with respect to earth horizontal
σ	standard deviation or band within which 68 percent of the data falls

ω   ratio of secondary total
temperature at exit of
secondary passage to pri-
mary total temperature

ratio of secondary to pri-
mary weight flows

REFERENCES

1. Mikkelson, D. C. and Head, V. L., "Flight In-
vestigation of Airframe Installation Effects
on a Variable Flap Ejector Nozzle of an
Underwing Engine Nacelle at Mach Numbers
from 0.5 to 1.3," TM X-2010, 1970, NASA,
Cleveland, Ohio.

2. Beaulieu, W., Campbell, R., and Burcham, F. W.,
"Measurement of the XB-70A Propulsion Per-
formance Incorporating the Gas Generator
Method," Journal of Aircraft, Vol. 6, No. 4,
July-Aug. 1969, pp. 312-317.

3. Davidson, T W., "Method of Net Thrust Mea-
surement in Supersonic Flight," Aerodynamics
of Power Plant Installation, Agardograph 103,
Part I, Oct. 1965, pp. 217-243.

4. Waters, M. H. and Graham, P. A., "Evaluation of
an Exhaust Nozzle Traversing Rake System as
an In-Flight Thrust Measuring Device for an
Afterburning Turbofan Engine," NAPTC-ATD-159,
Nov. 1968, Naval Air Propulsion Test Center,
Trenton, N. J.

5. Samanich, N. E. and Huntely, S. C., "Thrust and
Pumping Characteristics of Cylindrical
Ejector Using Afterburning Turbojet Gas Gen-
erator," TM X-52569, 1969, NASA, Cleveland,
Ohio.

6. Antl, R. J. and Burley, R. R., "Steady State
Airflow and Afterburning Performance Char-
acteristics of Four J85-GE-13 Turbojet En-
gines," TM X-1742, 1969, NASA, Cleveland,
Ohio.

Type measurement	Estimated accuracy ~ 1 σ
Engine RPM	±0.25 percent full scale
Engine fuel flows	±0.75 percent full scale
Temperatures	±5° F
Pressures (scanivalve)	±0.5 percent full scale
Altitude	±100 ft
Mach number	±0.5 percent
Free stream total temperature	±2° F
Load cell	±0.25 percent full scale

TABLE 1

Parameter		Influence coefficient		Measurement accuracy ~percent	Error contribution ~percent	
		Tare coefficient	Ideal thrust		Tare coefficient	Ideal thrust
Measured engine and nozzle	Engine rpm	2.779	1.200	0.250	0.700	0.300
	Engine fuel flow	.051	.000	1.000	.051	.000
	Compressor face total pressure	2.450	.925	1.000	2.450	.925
	Turbine discharge pressure	.258	.306	1.000	.258	.306
	Turbine discharge temperature	1.201	.518	.285	.342	.147
	Secondary air temperature	.117	0	.620	.073	0
	Secondary valve area	.141	0	1.000	.141	0
	Inlet pressure to secondary valve	.054	0	1.000	.054	0
	Exit pressure at secondary valve	.072	0	1.000	.072	0
	Internal pressure at nozzle exit	0	0	1.000	0	0
	Base pressure on nozzle	1.166	0	1.150	1.340	0
	Load cell force	.660	0	1.000	.660	0
Calibration parameter	Nozzle thrust coefficient	2.738	0	0.250	0.686	0
	Engine airflow	2.274	.326	.300	.685	.098
	Secondary airflow	1.201	0	1.000	1.201	0
	Afterburner pressure drop	.014	.002	1.000	.014	.002
Free stream	Mach number	1.700	0.028	0.500	0.850	0.014
	Altitude	3.500	.340	.425	1.485	.144
	Total temperature	2.400	.845	.440	1.055	.372
				$\sum[(c_i)(\Delta x_i/x)]^2$	15.366	1.236
				E = Error	±3.920	±1.11

TABLE 2 MILITARY POWER, MACH 0.90

Parameter	Influence coefficient		Measurement accuracy	Error contribution ~percent	
	Tare coefficient	Ideal thrust		Tare coefficient	Ideal thrust
Measured engine and nozzle					
Engine rpm	2.631	0.867	0.250	0.658	0.217
Engine fuel flow	.117	.039	1.250	.146	.049
Compressor face total pressure	1.880	.925	1.000	1.880	.925
Turbine discharge pressure	.315	.312	1.000	.315	.312
Turbine discharge temperature	.445	.117	.285	.127	.033
Secondary air temperature	.070	0	.577	.041	0
Secondary valve area	.085	0	1.000	.085	0
Inlet pressure to secondary valve	.068	0	1.000	.068	0
Exit pressure at secondary valve	.075	0	1.000	.075	0
Inlet pressure at nozzle exit	.029	0	1.000	.029	0
Base pressure on nozzle	1.144	0	1.180	1.350	0
Load cell force	1.110	0	.825	.916	0
Calibrated parameters					
Nozzle thrust coefficient	3.020	0	1.500	4.530	0
Engine airflow	2.916	.966	.300	.875	.290
Secondary airflow	.137	0	1.000	.137	0
Afterburner pressure drop	.024	.024	1.000	.024	.024
Afterburner temperature rise	.483	.149	1.000	.483	.149
Free stream					
Mach number	1.700	0.028	0.500	0.850	0.014
Altitude	3.500	.340	.425	1.487	.144
Total temperature	2.400	.845	.440	1.056	.372
			$\Sigma[(c_i)(\Delta x_i/x)]^2$	32.374	1.270
			E = Error	±5.689	±1.127

TABLE 3   MINIMUM REHEAT, MACH 0.90

Parameter		Influence coefficient		Measurement accuracy	Error contribution ~percent	
		Tare co-efficient	Ideal thrust		Tare coeffi-cient	Ideal thrust
Measured engine and nozzle	Engine rpm	2.639	0.838	0.250	0.659	0.209
	Engine fuel flow	.197	.060	1.000	.197	.060
	Compressor face total pressure	1.670	.925	1.000	1.670	.925
	Turbine discharge pressure	.807	.341	1.000	.807	.341
	Turbine discharge temperature	.648	.255	.285	.185	.072
	Secondary air temperature	.078	0	.550	.043	0
	Secondary valve area	.129	0	1.000	.129	0
	Inlet pressure to secondary valve	.254	0	1.000	.254	0
	Exit pressure at secondary valve	.251	0	1.000	.251	0
	Internal pressure at nozzle exit	.026	0	1.000	.026	0
	Base pressure on nozzle	1.124	0	1.000	1.326	0
	Load cell force	1.585	0	.500	.792	0
Calibrated parameters	Nozzle thrust coefficient	3.640	0	1.500	5.460	0
	Engine airflow	2.940	.944	.300	.882	.283
	Secondary airflow	.160	0	1.000	.160	0
	Afterburner pressure drop	.074	.038	1.000	.074	.038
	Afterburner temperature rise	.811	.258	1.000	.811	.258
Free stream	Mach number	1.700	0.028	0.500	0.850	0.014
	Altitude	3.500	.340	.425	1.487	.144
	Total temperature	2.400	.845	.440	1.056	.372
					41.807	1.332
				$\bar{E} = \Sigma[(c_i)(\Delta x_i/x)]^2$		
				$\bar{E}$ = Error	±6.466	±1.154

TABLE 4   MAXIMUM REHEAT, MACH 0.90

Parameter	Influence coefficient, c_i	Accuracy, percent	Error contribution, percent	
Estimated nacelle tare	0.598	±3.920	±2.344	
Experimental nacelle tare	0.598	±1.500	±0.895	
Ideal thrust	0.994	±1.110	±1.101	
Load cell force	0.395	±1.000	±0.395	
		E =	±2.620	FOR ESTIMATED TARE
		E =	±1.473	FOR EXPERIMENTAL TARE USING TARE SCATTER

TABLE 5   ANALYSIS OF RANDOM ERROR IN NOZZLE EFFICIENCY MILITARY POWER, MACH 0.90

Parameter	Influence coefficient, c_i	Accuracy, percent	Error contribution, percent	
Estimated nacelle tare	0.435	±3.920	±1.712	
Experimental nacelle tare	0.435	±1.500	±0.652	
Ideal thrust	0.993	±1.127	±1.119	
Load cell force	0.5432	±0.825	±0.447	
		E =	±2.088	FOR ESTIMATED TARE
		E =	±1.370	FOR EXPERIMENTAL TARE USING TARE SCATTER

TABLE 6   ANALYSIS OF RANDOM ERROR IN NOZZLE EFFICIENCY MINIMUM REHEAT, MACH 0.90

Parameter	Influence coefficient, C_i	Accuracy, percent	Error contribution, percent	
Estimated nacelle tare	0.366	±3.920	±1.435	
Experimental nacelle tare	0.366	±1.500	±0.550	
Ideal thrust	0.989	±1.154	±1.141	
Load cell force	0.636	±0.500	±0.318	
		E =	±1.861	FOR ESTIMATED TARE
		E =	±1.306	FOR EXPERIMENTAL TARE USING TARE SCATTER

TABLE 7 ANALYSIS OF RANDOM ERROR IN NOZZLE EFFICIENCY MAXIMUM AFTERBURNER, MACH 0.90

Most significant parameters	Influence coefficient, C_i		Measurement accuracy $\Delta X_i/X_i$ ~percent	Error contribution ~percent	
	Tare coefficient	Ideal thrust		Tare coefficient	Ideal thrust
ENGINE AND LOAD CELL					
Engine rpm	2.779	1.200	0.250	0.700	0.300
Compressor face pressure	2.450	.925	1.000	2.450	.925
Turbine discharge temperature	1.201	.518	.285	.203	.147
Load cell force	.660	0	1.000	.660	0
CALIBRATIONS					
Nozzle thrust coefficient	2.738	0	0.250	0.686	0
Engine airflow	2.274	.326	.300	.685	.098
FREE STREAM					
Mach number	1.700	0.028	0.500	0.850	0.014
Altitude	3.500	.340	.425	1.485	.144
Free stream total temperature	2.400	.845	.440	1.055	.372

$$\text{Error} = \sqrt{\left[\sum\left(C_i\,\frac{\Delta X_i}{X_i}\right)\right]^2} = \pm 3.9 \text{ percent for tare coefficient}$$
$$= \pm 1.1 \text{ percent for ideal thrust}$$

ERROR ANALYSIS, MILITARY POWER, MACH 0.90

Most significant parameters	Influence coefficient, C_i		Measurement accuracy $\Delta X_i/X_i$ ~percent	Error contribution ~percent	
	Tare coefficient	Ideal thrust		Tare coefficient	Ideal thrust
ENGINE AND LOAD CELL					
Engine rpm	2.639	0.838	0.250	0.659	0.209
Compressor face pressure	1.670	.925	1.000	1.670	.925
Turbine discharge temperature	.648	.255	.285	.185	.072
Load cell force	1.585	0	.500	.792	0
CALIBRATIONS					
Nozzle thrust coefficient	3.640	0	1.500	5.460	0
Engine airflow	2.940	.944	.300	.882	.283
FREE STREAM					
Mach number	1.700	0.028	0.500	0.850	0.014
Altitude	3.500	.340	.425	1.487	.144
Free stream total temperature	2.400	.845	.440	1.056	.372

$$\text{Error} = \sqrt{\left[\sum\left(C_i\,\frac{\Delta X_i}{X_i}\right)\right]^2} = \pm 6.4 \text{ percent for tare coefficient}$$
$$= \pm 1.11 \text{ percent for ideal thrust}$$

ERROR ANALYSIS, MAXIMUM REHAT, MACH 0.90
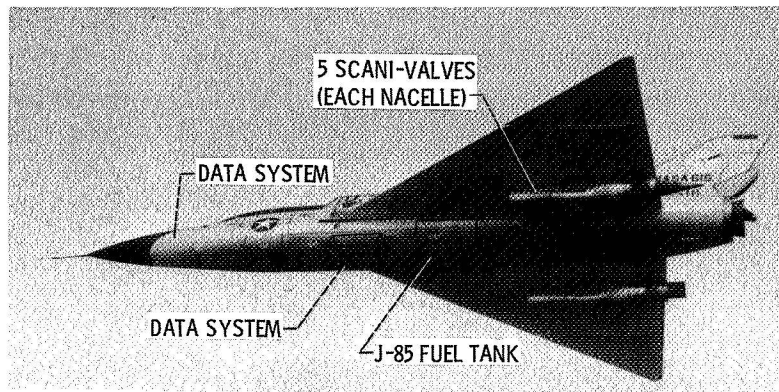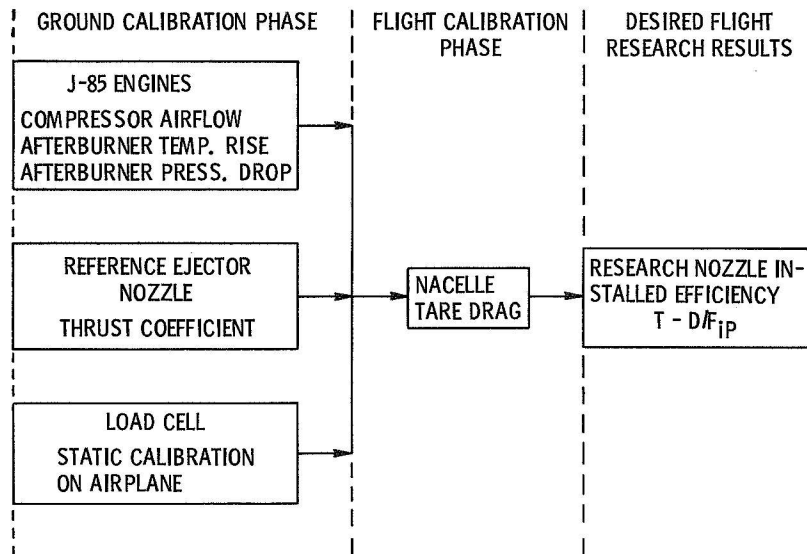
Figure 1. - Modified F-106.

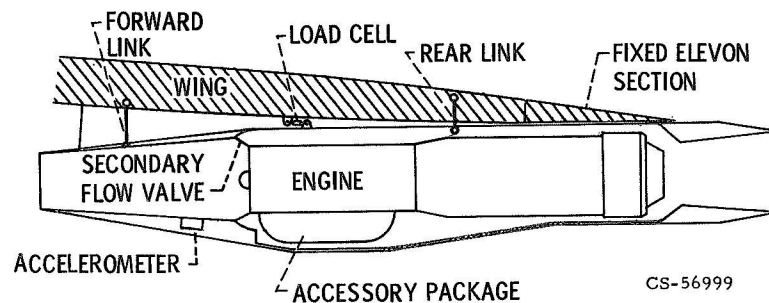Figure 2. - Method of obtaining nozzle performance.
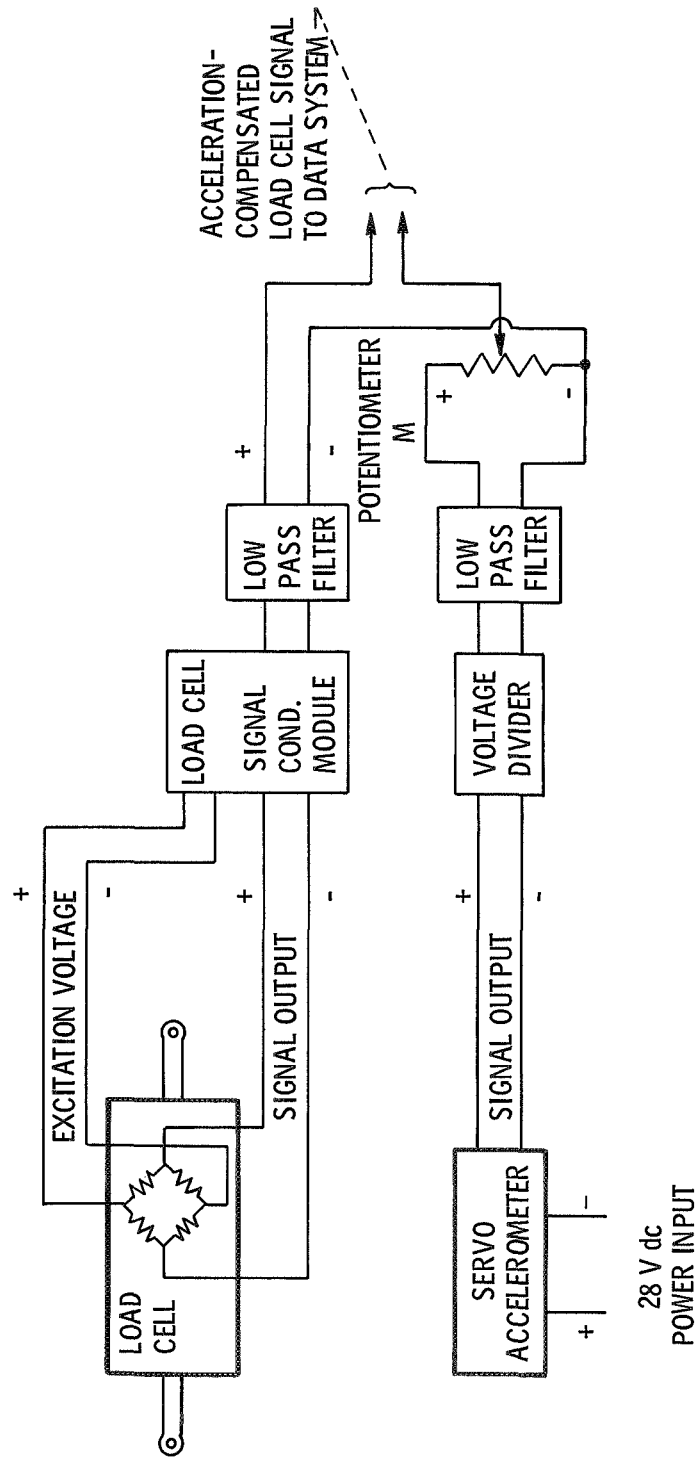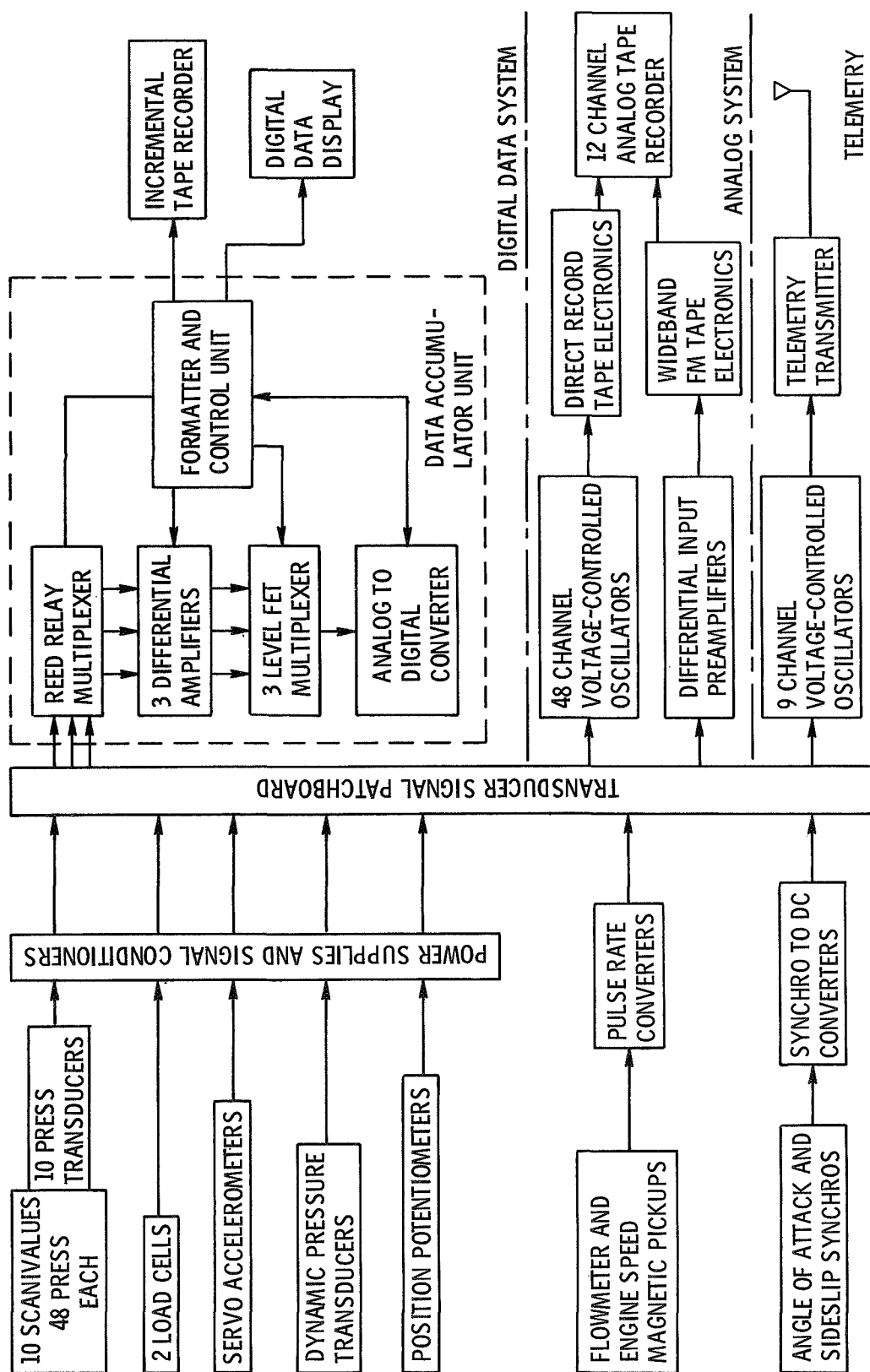

Figure 3. - Nacelle-engine installation.
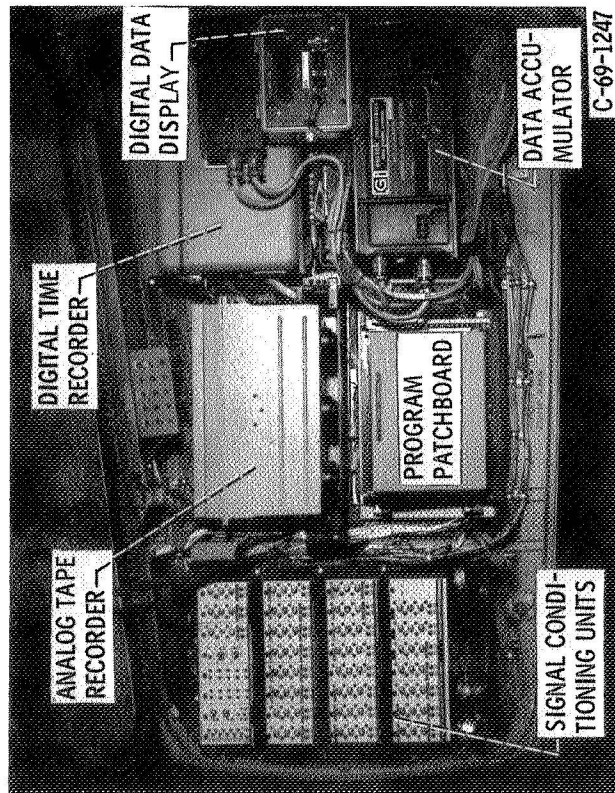
Figure 4. - Load cell compensation schematic.

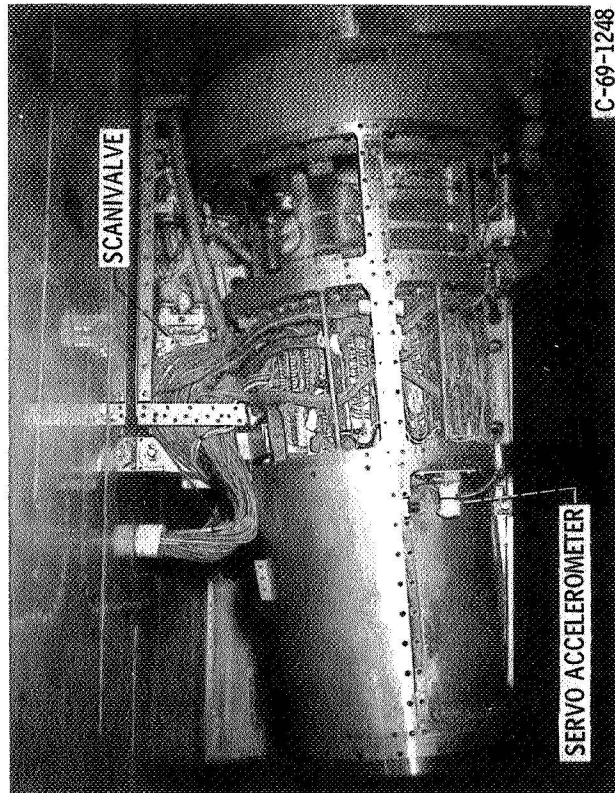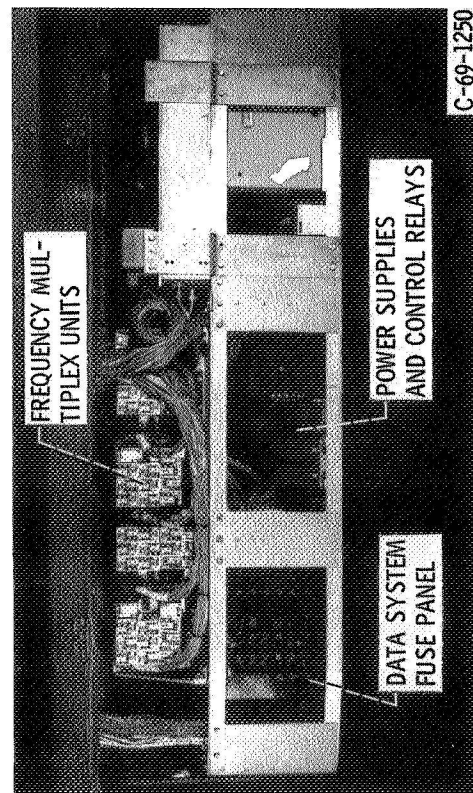Figure 5. – Data acquisition system schematic.

E - 6287

SCANIVALVE

SERVO ACCELEROMETER

C-69-1248

(b) Left nacelle inlet with cover panels removed.

THROTTLE SERVO-VALVE AMPLIFIER

ANALOG PRE-AMPLIFIER

SCANIVALVE CONTROLLER

DATA SYSTEM CONTROL UNIT

C-69-1249

(d) Left side missile bay rack, lowered.

DIGITAL DATA DISPLAY

DIGITAL TIME RECORDER

ANALOG TAPE RECORDER

PROGRAM PATCHBOARD

DATA ACCU-MULATOR

SIGNAL CONDI-TIONING UNITS

C-69-1247

(a) Left forward electronics compartment (nose).

FREQUENCY MUL-TIPLEX UNITS

POWER SUPPLIES AND CONTROL RELAYS

DATA SYSTEM FUSE PANEL

C-69-1250
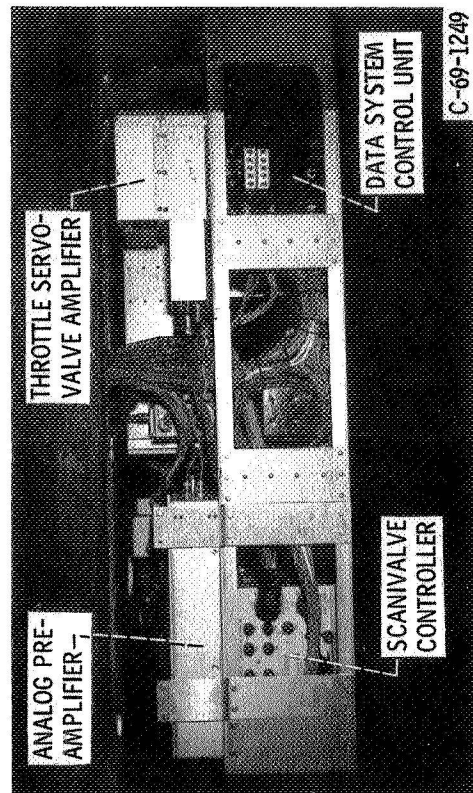
(c) Right side missile bay rack, lowered.

Figure 6. - Data acquisition system components.

TURBINE DISCHARGE
TOTAL PRESSURE

kN/m^2 abs (PSIA)

	kN/m^2 abs	(PSIA)
————————	241.2	(35)
—— ——	206.9	(30)
— — — —	137.9	(20)
—·— —·—	68.9	(10)
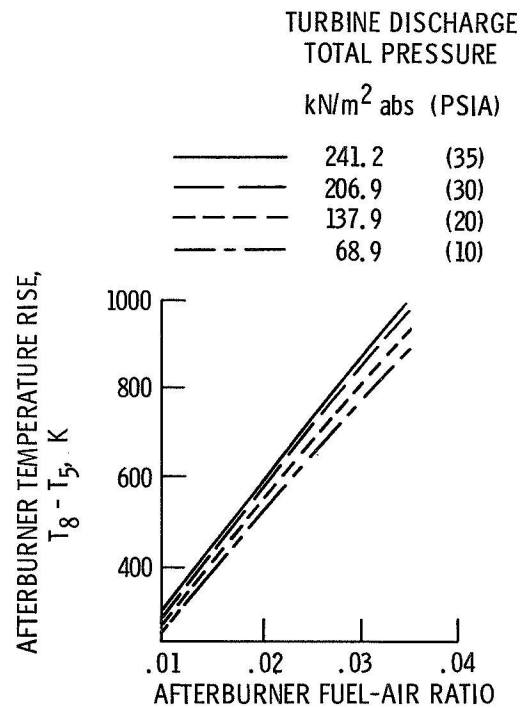
Figure 7. - J-85 engine after-
burner calibration.
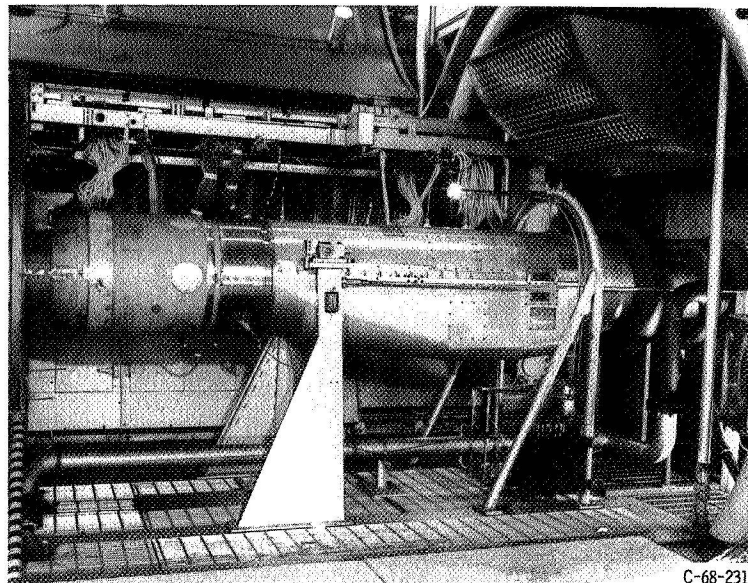
C-68-2311

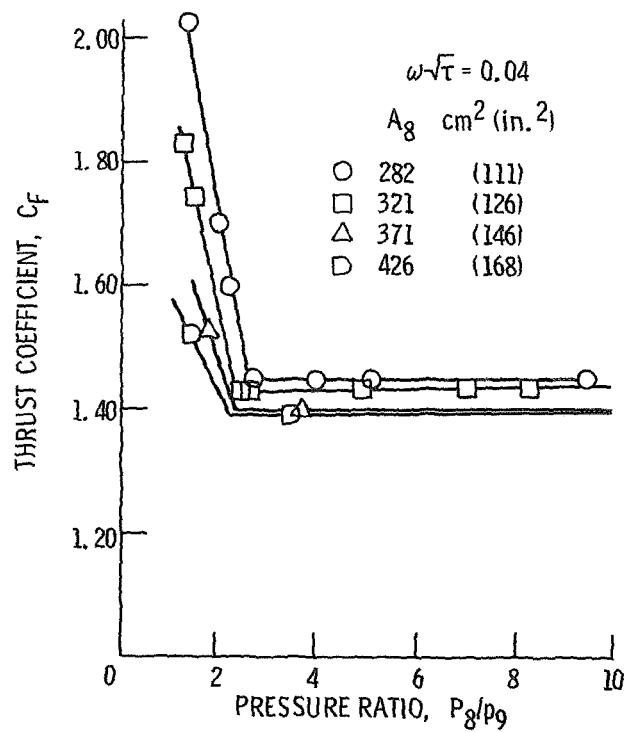Figure 8. - Propulsion Systems Laboratory's test nacelle.
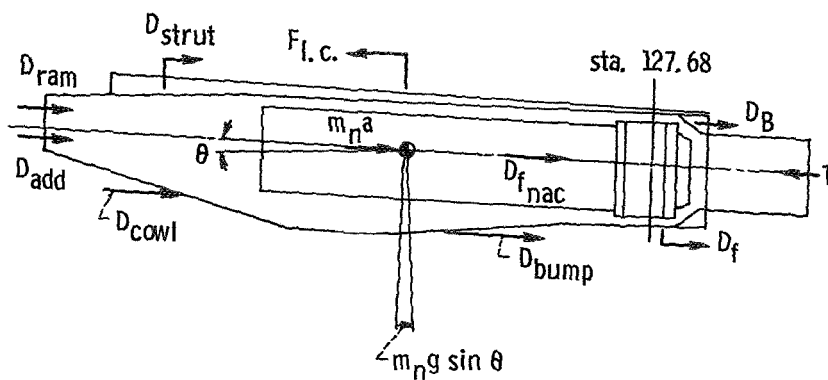
Figure 9. - Nacelle forces.
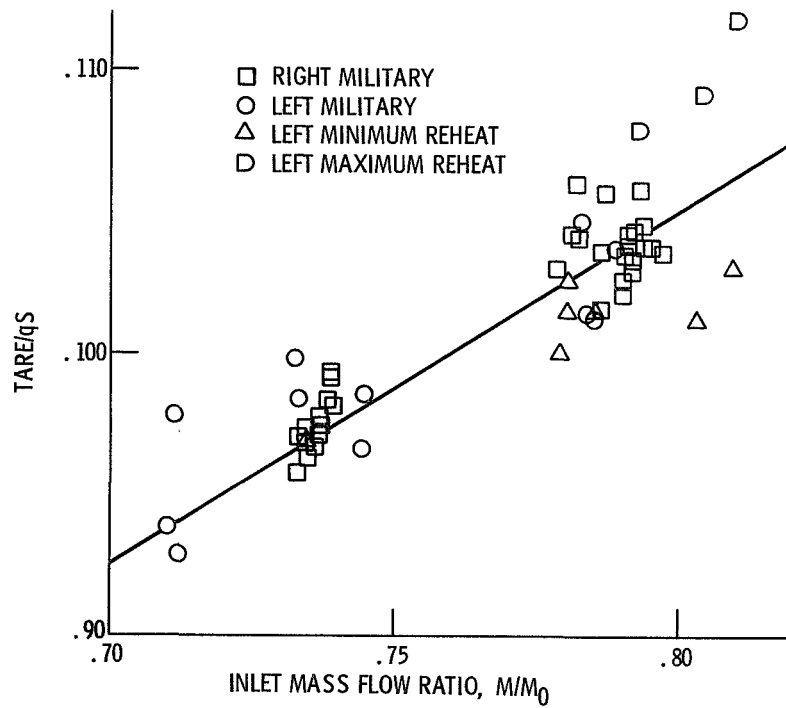

Figure 10. - Reference nozzle thrust calibration.
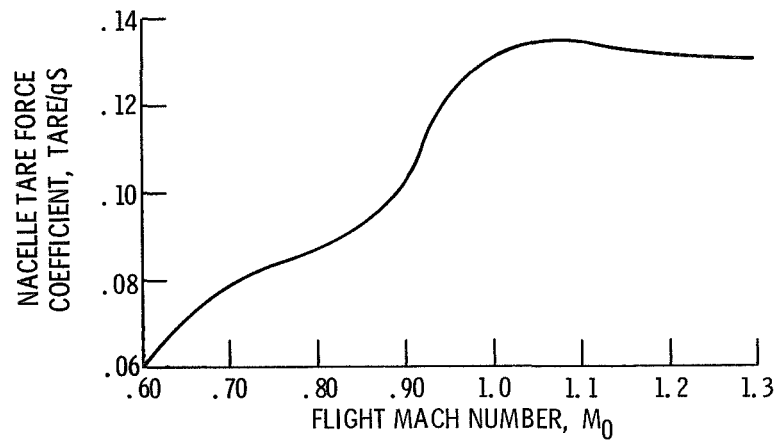
Figure 11. - Mach number, 0.90.

Figure 12. - Tare coefficient variation with Mach number, at a constant mass flow ratio, 0.82.
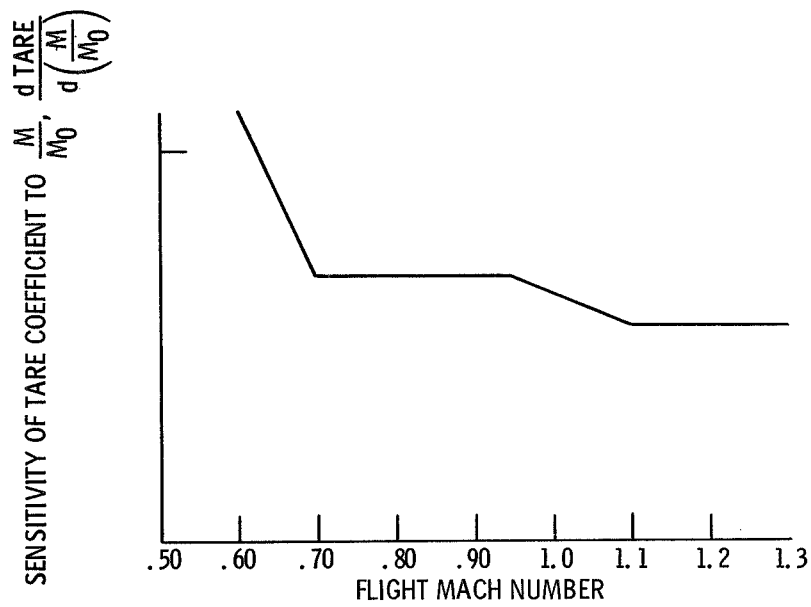
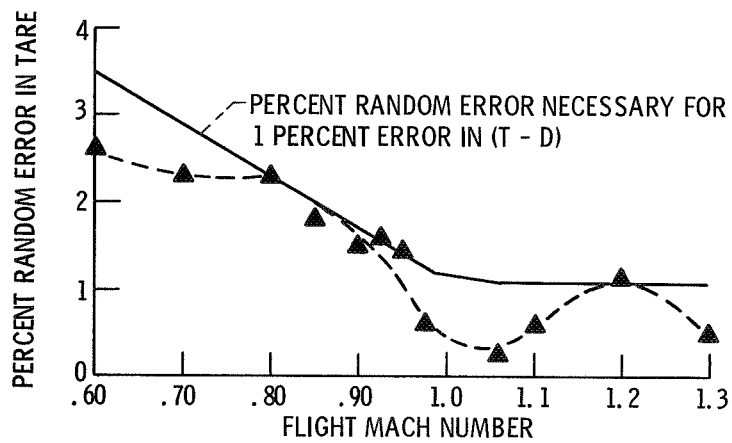Figure 13. - Change of take coefficient with mass flow ratio.

Figure 14. - Percent random error in tare versus flight Mach number, for military power.
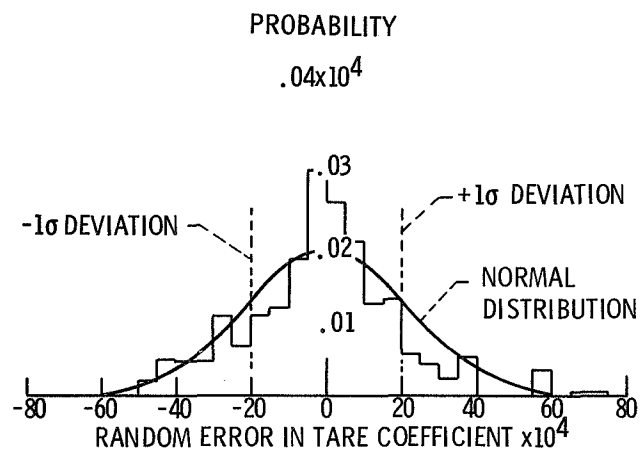
PROBABILITY

$.04 \times 10^4$

Figure 15. – Probability distribution of military data.